International Journal of Nanomedicine

Dovepress
open access to scientific and medical research

Open Access Full Text Article

ORIGINAL RESEARCH

# pH-sensitive strontium carbonate nanoparticles as new anticancer vehicles for controlled etoposide release



This article was published in the following Dove Press journal:
International Journal of Nanomedicine
19 November 2012
Number of times this article has been viewed

Wen-Yu Qian[1,*]
Dong-Mei Sun[1,*]
Rong-Rong Zhu[1]
Xi-Ling Du[1]
Hui Liu[2]
Shi-Long Wang[1]

[1]Shanghai Tenth People's Hospital, School of Life Science and Technology, Tongji University, Shanghai, PR China; [2]Eastern Hepatobiliary Surgery Hospital, Second Military Medical University, Shanghai, PR China

*Wen-Yu Qian and Dong-Mei Sun contributed equally to this work

**Abstract:** Strontium carbonate nanoparticles (SCNs), a novel biodegradable nanosystem for the pH-sensitive release of anticancer drugs, were developed via a facile mixed solvent method aimed at creating smart drug delivery in acidic conditions, particularly in tumor environments. Structural characterization of SCNs revealed that the engineered nanocarriers were uniform in size and presented a dumbbell-shaped morphology with a dense mass of a scale-like spine coating, which could serve as the storage structure for hydrophobic drugs. Chosen as a model anticancer agent, etoposide was effectively loaded into SCNs based on a simultaneous process that allowed for the formation of the nanocarriers and for drug storage to be accomplished in a single step. The etoposide-loaded SCNs (ESCNs) possess both a high loading capacity and efficient encapsulation. It was found that the cumulative release of etoposide from ESCNs is acid-dependent, and that the release rate is slow at a pH of 7.4; this rate increases significantly at low pH levels (5.8, 3.0). Meanwhile, it was also found that the blank SCNs were almost nontoxic to normal cells, and ESCN systems were evidently more potent in antitumor activity compared with free etoposide, as confirmed by a cytotoxicity test using an MTT assay and an apoptosis test with fluorescence-activated cell sorter (FACS) analysis. These findings suggest that SCNs hold tremendous promise in the areas of controlled drug delivery and targeted cancer therapy.

**Keywords:** strontium carbonate, nanoparticles, pH-sensitive drug delivery, etoposide, anticancer activity

## Introduction

Nanocarriers for drug delivery have become key vehicles for the storage and delivery of drugs, especially anticancer drugs, because their small size enables them to leave the leaky tumor vasculature and accumulate at the tumor site through an enhanced permeability and retention (EPR) effect.[1–3] Various nanocarriers including liposomes, polymers, micelles, dendrimers, gold, iron oxide, carbon-based materials, and silicon have been developed and explored as vehicles for the controlled release of anticancer drugs.[4–13] However, most of the existing anticancer agents cannot distinguish between cancerous and healthy cells, leading to toxic actions and side effects. To further improve drug delivery efficiency and cancer specificity, tumor-targeting strategies have recently received significant attention.[14,15]

One of the most promising tumor targeting approaches is the investigation of pH-sensitive drug delivery systems, as the existing pH of tumor tissue is generally considered an ideal trigger for the selective release of anticancer drugs.[16,17] Compared to normal tissue (pH 7.4), the average extracellular pH value in tumor tissues is 6.8, and the pH values of intracellular components such as endosomes and lysosomes are 4.5–6.5, which

Correspondence: Shi-long Wang
Shanghai Tenth People's Hospital, School of Life Science and Technology, Tongji University, 1239 Siping Road
Shanghai 200092, PR China
Tel +86 21 659 825 95
Fax +86 21 659 822 86
Email wsl@tongji.edu.cn

Hui Liu
Eastern Hepatobiliary Surgery Hospital, Second Military Medical University, Shanghai 200438, PR China
Tel +86 21 818 754 63
Fax +86 21 655 624 00
Email liuhuigg@hotmail.com

is caused by hypoxia in poorly perfused regions due to the high metabolic rate required for tumor growth.[18] The specificity of lower pH levels within the tumor region can be a strategy for acid-sensitive drug delivery at local microenvironments for not only improving the efficacy of chemotherapy, but also for reducing the level of cytotoxicity.

Recent studies have highlighted the development of some drug carriers with pH-sensitive, and therefore tumor-selective, drug delivery. Johnson et al,[19] Lin and Kim,[20] Li et al[21] (micelles), Deng et al[22] (chitosan-silica nanospheres), and Jin et al[23] (polymers) all introduced new pathways for developing acid-response drug delivery systems. However, most of the pH-sensitive materials reported were organic-based, which may be less biocompatible, involve complicated manufacturing, and usually limit drug payloads (less than 15%). To circumvent these problems, the strategy of the present paper is to take advantage of the character and performance of inorganic materials in developing a targeted drug delivery system for anticancer drugs.

Inorganic nanocarriers as drug delivery vehicles have been investigated extensively in the past decade,[24–28] and some of their benefits stem from their versatile properties such as being widely available, rich in functionality, offering favorable biocompatibility, and requiring mild preparation conditions; this field of research is further reinforced with continuous development of various new nanocarriers. Currently, many inorganic materials are being used for inorganic drug delivery (for instance, carbon materials, calcium phosphate, layered double hydroxide, gold, iron oxide, and silicon oxide[29–34]), but for the most part these initiatives have been unsatisfactory. Critical properties of inorganic nanocarriers include nonbiodegradability, high leakage of drugs, and poor cellular internalization, which affect their efficiency in drug delivery. New strategies are therefore desired to address these limitations.

Here, we introduced strontium carbonate nanoparticles (SCNs) as nanocarriers for controlled drug delivery. Strontium (Sr), in human biology and pathology, has attracted less attention than the other two important divalent metals, calcium and magnesium. Although this is still true, there is an increasing awareness of the biological role of Sr after the development of the drug strontium ranelate, which has recently been shown to be an effective medication in the treatment of osteoporosis.[35,36] Though a biomimetic system supported liquid membrane for obtaining SCNs was studied by Sun et al,[27] few articles reported on the synthesis of SCNs. In this article, we initially came up with an in situ, single step, synchronous method for both the synthesis of SCNs and the loading of the hydrophobic drug into SCN carriers in mixed solvents. Using the facile method, nontoxic SCNs of uniform size have been synthesized for biological applications. The samples were characterized, and their high efficiency as drug carriers was tested with a challenging anticancer drug, etoposide, which is generally applied, but has shown poor bioavailability in gastric cancer chemotherapy.[37] It appeared as though the pH-sensitivity of SCNs yielded an improved performance in delivering the drug, suggesting that SCNs are innovative carriers for drug delivery.

# Materials and methods

## Materials

Etoposide (≥98%), dimethyl sulfoxide (DMSO), and MTT Formazan were purchased from Sigma Chemical Co (St Louis, MO). $SrCl_2 \cdot 6H_2O$ (AR), $Na_2CO_3$ (AR), citric acid (AR), HCl (36%–38%), and ethanol (AR) were purchased from Sinopharm Chemical Regent Co, Ltd (Shanghai, China). All the chemicals were used as received without further purification. Dulbecco's modified Eagle's medium (high glucose), RPMI-1640, fetal calf serum, penicillin G, streptomycin, and trypsinase were obtained from Gibco-BRL (Life Technologies Corporation, Grand Island, NY).

## Preparation of etoposide-loaded strontium carbonate nanoparticles

All of the experiments were conducted at room temperature (about 15°C–25°C). In a typical procedure, the etoposide-loaded strontium carbonate nanoparticles (ESCNs) were prepared using 0.837 g of etoposide and 0.267 g $SrCl_2 \cdot 6H_2O$, which were dissolved in a 180 mL mixed solvent of ethanol and deionized water (volume ratio = 8:1), marked as Solution A. A total of 0.106 g $Na_2CO_3$ was dissolved in a 40 mL mixed solvent of ethanol and deionized water (volume ratio = 1:1), marked as Solution B. After 0.026 g citric acid was added into Solution A, Solution B was added drop-wise to the vigorously stirred Solution A and reacted for 24 hours. The product was centrifuged, washed thrice with deionized water, and dried at 60°C. The blank carrier strontium carbonate nanoparticles (SCNs) were prepared without the addition of etoposide, and other experimental parameters used were similar to that of the ESCNs sample.

## Characterization

The spatial and morphological studies were carried out with field emission scanning electron microscopy (S4800; Hitachi Ltd, Tokyo, Japan) at an accelerating voltage of 1–5 kV. The crystallographic structure of the solid samples was determined with X-ray diffraction (XRD,

Bruker D8; Bruker AXS, Inc, Madison, WI) with Cu Kα radiation (λ = 0.154056 nm, 40 kV, 40 mA, step of 0.0330°). The average particle size (z-average size) and size distribution were measured using photon correlation spectroscopy (LS230, Beckman Coulter Inc, Brea, CA) at 25°C under a fixed angle of 90° in disposable polystyrene cuvettes. The measurements were conducted using a He-Ne laser of 633 nm. Fourier transform infrared spectra were obtained on a Bruker Vector 22 (Bruker AXS, Inc) spectrophotometer in the range of 4000–400 $cm^{-1}$ using the standard KBr disk method (sample/KBr = 1/100). Ultraviolet-visible (UV-vis) spectra were measured on a Cary 50UV-visible absorbance spectrophotometer (Varian, Victoria, Australia).

## Sedimentation study in phosphate-buffered solution (PBS)

A total of 10 mg of etoposide was placed in a microcentrifugal tube of 1.5 mL and resuspended with 1 mL of PBS. The tube then stood for over 8 hours after vortexing for 1 minute. Photographs of the sample were taken at 10 minutes, 3 hours, and 8 hours, respectively. Other samples were studied in the same way. Based on the drug encapsulation efficiency, the same quantity of etoposide was applied to all formulations for the sedimentation study.

## Evaluation of the buffer effect

The pH, which changes in each suspension after the addition of 0.1 M HCl aqueous solution, was recorded to measure the buffer effect of prepared samples. HCl aqueous solution was subsequently added to the suspension (10 mL) containing the prepared sample (100 mg), and was continuously stirred at 37°C, until the pH dropped to an approximate value of 2.5.

## Determination of loading amount and in vitro release test

The amount of entrapped etoposide was determined by UV-vis spectroscopy. An ESCN sample of a standard weight was placed in a 10 mL flask, then 1 mL of 3 M HCl solution was added into it, and the flask was filled with 0.02 M of PBS (pH 7.4) until the total volume reached 10 mL. After the ESCNs sample was totally dissolved, the concentration of etoposide was determined with a UV-vis spectrophotometer. The selected wavelength used for the measurement of the etoposide was 285 nm. The concentration of the etoposide was calculated according to an already obtained calibrating curve (Abs = 0.00746c + 0.000967, r = 0.99985). The drug-loading capacity and encapsulation efficiency are calculated by:

$$\text{Drug} - \text{Loading capacity} = \frac{\text{Weight of etoposide in ESCNs}}{\text{Weight of ESCNs}} \times 100\%$$

$$\text{Drug encapsulation efficiency} = \frac{\text{Weight of etoposide in ESCNs}}{\text{Weight of etoposide fed initially}} \times 100\%$$

The etoposide release test was performed as follows: 100 mg of ESCNs were resuspended in 5 mL of PBS at pH 7.4, pH 5.8, and pH 3.0. A dialysis bag was pretreated with ethylenediaminetetraacetic acid, loaded with the sample, placed in a flask of 500 mL with 200 mL of PBS at same pH value, and swayed in a bath-reciprocal shaker at 100 rpm at 37°C over 72 hours. A total of 1 mL of the fluid containing the released etoposide was extracted at desired time intervals, and another 1 mL of fresh PBS was added to the medium. The accumulated amount of released etoposide was determined by UV absorption at 285 nm.

## Cytotoxicity assay

Human embryonic kidney (HEK) 293T cells with a density of $1 \times 10^4$ cells/well were seeded on a 96-well polystyrene plate, and each well contained 100 μL of Dulbecco's modified Eagle's medium (high glucose) supplemented with 10% fetal bovine serum and a 1% penicillin-streptomycin solution. After incubation at 37°C in a 5% $CO_2$ humid environment for 24 hours, triplicate wells were treated with SCNs, free etoposide, and ESCNs in different concentrations of 5, 10, 20, and 40 μg/mL. These HEK293T cells were incubated as described above for 24 and 48 hours, respectively. Cells did not treat with any agents served as a blank control. The number of living cells was determined by MTT assay with 3-(4,5-dimethyl-thiazole-2-yl)-2,5-phenyltetrazolium bromide. After cells were incubated with 20 μL of MTT (5 mg/mL) for 4 hours at 37°C under a light-blocking condition, the medium was removed and 150 μL of DMSO was added into each well. Absorbance was measured at 490 nm using the ELx800 reader (BioTek Instruments, Inc, Winooski, VT), and cell viability was calculated by:

$$\text{Cell viability}\,(\%) = \frac{OD_{490}(\text{test}) - OD_{490}(\text{blank})}{OD_{490}(\text{control}) - OD_{490}(\text{blank})} \times 100\%$$

## Inhibition against SGC-7901 cells

Human gastric carcinoma (SGC-7901) cells with a density of $8 \times 10^4$ cells/well were seeded on a 96-well polystyrene plate; each well contained 100 μL of Roswell Park Memorial Institute 1640 medium supplemented with 10% fetal bovine serum and 1% penicillin-streptomycin solution. After incubation at

37°C in 5% $CO_2$ humidity for 24 hours, triplicate wells were treated with SCNs, free etoposide, and ESCNs in different concentrations of 5, 10, 20, and 40 μg/mL. Based on the drug encapsulation efficiency, the same quantity of etoposide was applied to all formulations for the growth inhibition study. These HEK293T cells were incubated as described above for 24 and 48 hours, respectively. A control experiment was performed without treated under the same conditions. A total of 20 μL (5 mg/mL) of MTT dye solution was added to each well before the cells were incubated for 4 hours at 37°C under a light-blocking condition. The medium was then removed and 150 μL of DMSO was added into each well. Absorbance was measured at 490 nm using an ELx800 reader (BioTek Instruments, Inc, Winooski, VT), and inhibition against SGC-7901 cells was calculated by:

$$\text{Inhibition}(\%) = \left[1 - \frac{OD_{490}(\text{test}) - OD_{490}(\text{blank})}{OD_{490}(\text{control}) - OD_{490}(\text{blank})}\right] \times 100\%$$

## Fluorescence activated cell sorter (FACS) analysis

The number of apoptotic cells was determined with the Annexin V-PI Detection KIT (keyGEN, Nanjing, China). SGC-7901 cells with a density of $1 \times 10^6$ cells/well were seeded on a 24-well polystyrene plate suspended in RPMI-1640 with 10% pasteurized fetal calf serum and incubated for 24 hours at 37°C. The free etoposide, ESCNs, and culture medium were only added to each group at a concentration of 10 μg/mL. Based on the drug encapsulation efficiency, the same quantity of etoposide was applied to all formulations for the apoptosis analysis. The incubation continued for 24 hours at 37°C. The cells were then harvested and washed with PBS, and propidium iodide (PI) and annexin V were added directly to the cells suspended in the binding buffer (10 mM HEPES, 140 mM NaCl, 2.5 mM $CaCl_2$, pH 7.4). The cells were incubated in the dark for 15 minutes at 37°C and were submitted to FACS analysis on a Becton-Dickinson (Becton, Dickinson and Company, Mountain View, CA) spectrophotometer.

## Results and discussion

As shown in Figure 1, the synthetic scheme of ESCNs (SEM images shown in Figure 2) for drug delivery has been proposed. A mixed solvent method was employed to enable the simultaneous achievement of facilitated preparation for nanoscale particles,[38] and a high concentration of a hydrophobic drug (etoposide) could be made since ethanol was involved. Citric acid was used here as a crystal modifier to control the selectivity of polymorph and crystal morphology during the process of mineralization. After ionization, citric acid produces $H^+$ ions, which meet with $HCO_3^-$ ions, and then generate $CO_2$ and $H_2O$. The $CO_2$ bubble acts not only as the reactive material (hydrated and transformed into $CO_3^{2-}$ ions and $H^+$ ions), but also as the template of engineered nanoparticles, for the newly formed primary particles can attach to $CO_2$ bubbles and have their crystal forms modified (reaction formulas listed below). As a result, dumbbell-shaped SCNs have been prepared (SEM images shown in Figure 2). These nanoparticles present a dense mass of scale-like spine coating, which can easily entrap the drug in large amounts in a rapid stirring synthetic system

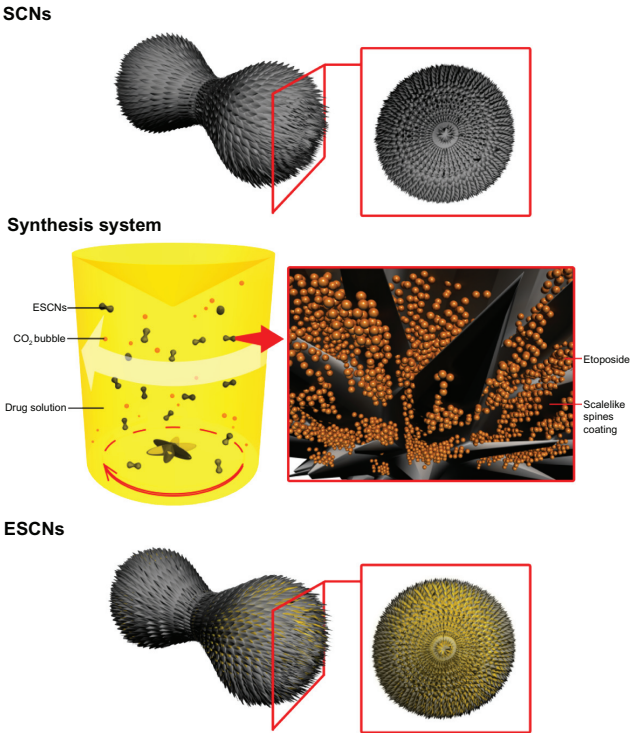


**Figure 1** A representative illustration of the synthesis system and SCNs before or after drug loading.
**Abbreviations:** SCNs, strontium carbonate nanoparticles; ESCNs, etoposide-loaded strontium carbonate nanoparticles.

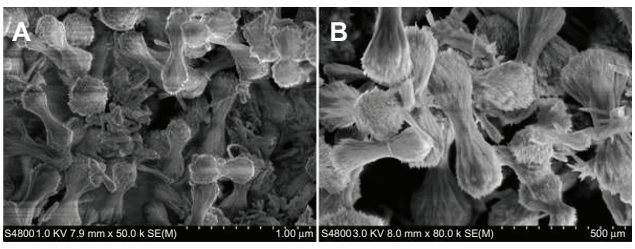


**Figure 2** SEM images of engineered SCNs with different enlarging ratios.
**Abbreviations:** SEM, scanning electron microscope; SCNs, strontium carbonate nanoparticles.

during and after the crystallization of SCNs. Accordingly, the synthesis of ESCNs was based on a simultaneous process of both nanocarrier formation and drug storage, which was accomplished in a single step.

$$2RCOOH(aq) + CO_3^{2-} = 2RCOO^- + H_2O(aq) + CO_2(g)$$

$$CO_2(g) \rightleftarrows CO_2(aq)$$

$$CO_2(aq) + H_2O(aq) \rightleftarrows HCO_3^- + H^+$$

$$HCO_3^- \rightleftarrows H^+ + CO_3^{2-}$$

$$Sr^{2+} + CO_3^{2-} = SrCO_3(s)$$

The morphology of the dumbbell-shaped nanoparticles of uniform size with good dispersal properties synthesized via the mixed solvent method is shown in Figure 2. It can be observed that the engineered SCNs present a dense mass of a scale-like spine coating, which can serve as the storage structure for hydrophobic drugs and prevent them from leaking out of the nanovehicles. The subunit's distribution size of engineered SCNs is narrow, with a nominal mean hydrodynamic diameter of 86.8 nm (image shown in Figure 4). All of these typical features of SCNs make them promising for biological applications.

The curve in Figure 3 shows the XRD pattern of prepared SCNs crystals, as well as a standard XRD pattern of $SrCO_3$. All diffraction peaks of the prepared products can be readily indexed to a pure orthorhombic phase of strontianite with lattice constants a = 5.107 Å, b = 8.414 Å, and c = 6.209 Å (data from JCPDS file number 05-0418). In addition, diffraction peaks of SCNs broadened due to a nanosize effect, and

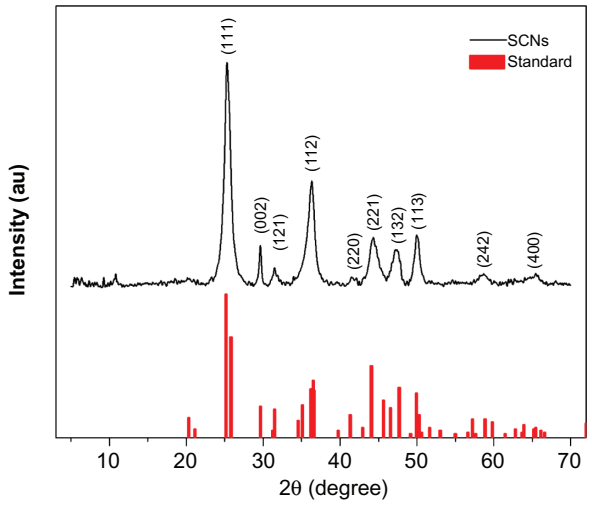


**Figure 3** XRD pattern of engineered SCNs and standard pattern of $SrCO_3$ (JCPDS 05-0418).
**Abbreviations:** XRD, X-ray diffraction; SCNs, strontium carbonate nanoparticles.

no additional peaks of other phases were found, indicating that the SCNs have been well crystallized and are of high purity.

UV-vis spectra of SCNs, etoposide, and ESCNs were obtained. The absorption curves of all samples incubated in 1 M HCl solution for 24 hours are shown in Figure 5. It was found that the curve of etoposide shows the characteristic absorption peak at approximately 285 nm, similar to what has been reported in the literature.[39] From the spectra of ESCNs, it can be observed that an obvious absorption emerged at 285 nm, which revealed that the carriers of ESCNs degraded in the acidic condition after 24 hours, releasing etoposide out in the solution. This suggests that etoposide was likely packed in the dense scale-like spine structure of the SCNs. In comparison, no absorption peaks were shown in the spectra of SCNs at 285 nm.

As shown in Figure 6, the Fourier transform infrared spectra of the sample etoposide (a), ESCNs (b), and SCNs (c) were obtained. The bands noted around 3400 $cm^{-1}$ were derived from the band vibration of O–H. The spectra of SCNs (c) displayed two strong absorption bands at 856 $cm^{-1}$ and 1465 $cm^{-1}$, which are characteristic bands of $SrCO_3$, which are in agreement with the results shown in the XRD patterns. The spectra of etoposide (a) show the following selected bands: 2923 $cm^{-1}$ (C–H stretch), 1770 $cm^{-1}$ (C=O stretch of ester bond), 1613 $cm^{-1}$ (C=O stretch of carboxyl methyl), and 1056 $cm^{-1}$ (C–O–C stretch), as well as the bands at 1487 $cm^{-1}$ and 1405 $cm^{-1}$, which correspond to the C=C stretching in the backbone of the aromatic phenyl ring. Compared with that of SCNs and etoposide, the spectra of ESCNs (b) present the characteristic bands of $SrCO_3$ (at 1487 $cm^{-1}$ and 860 $cm^{-1}$), with small shifts, indicating that the existence of pure $SrCO_3$ in the engineered nanohybrid remained unchanged. Moreover, the presence of almost all of the vibrations in the curve that are characteristic of etoposide (c) makes it clear that the etoposide was successfully packed into the SCNs, which may be consistent with the results highlighted in Figure 5.

Figure 7 presents the photographs of SCNs, etoposide, and ESCNs in double distilled water ($ddH_2O$), which were recorded at 10 minutes, 3 hours, and 8 hours after standing. As shown in Figure 7, both SCNs and ESCNs dispersed stably in $ddH_2O$, and hardly any sedimentation of the particles was observed after standing for 8 hours. In contrast with nanoagents, the free etoposide added in $ddH_2O$ began to be precipitated and aggregated in the initial 10 minutes, while most of the sample remained sedimentary at the bottom of the tube after standing for 8 hours, even though there was a trace

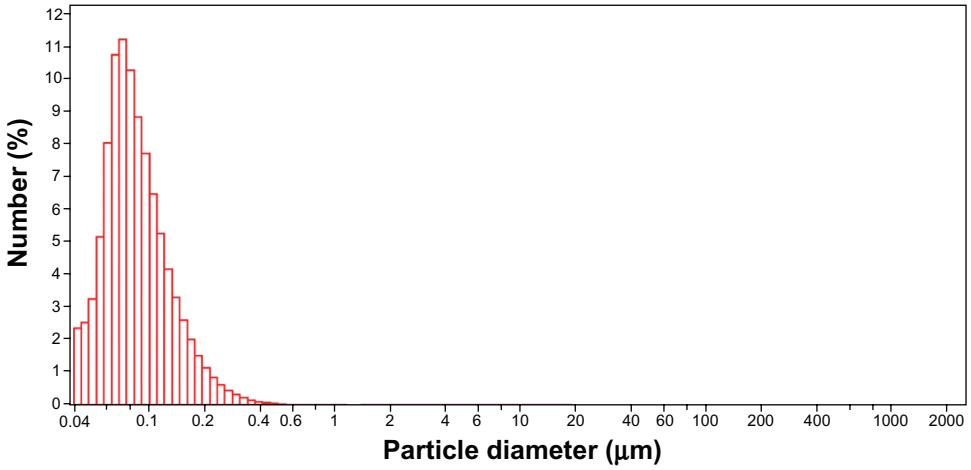


**Figure 4** Particle size distribution of SCNs.
**Abbreviation:** SCNs, strontium carbonate nanoparticles.

amount of dissolution. Therefore, the embedding of etoposide into SCNs is an effective means of improving the dispersion and stability of the drug in an aqueous suspension.

In our case, the ESCNs held both a high drug-loading capacity (34.4% ± 0.3%) and increased encapsulation efficiency (71.6% ± 1.9%). Since the therapeutic effectiveness of the drug is closely related to the release performance of the drug delivery system in the body, the in vitro release of the ESCNs was modeled in the different pH environments for blood and normal tissue (pH 7.4), tumor microenvironment (pH 5.8), in gastric juice (pH 3.0), and in three different buffered solutions for 72 hours at 37°C. The results are shown in Figure 8.

With the incremental release time, the amount of etoposide in the solution increased. In all chosen solutions, the drug release was fast during the first 24 hours. This may be attributed to the drug molecules that were packed in the structure of the dense scale-like spine coating of the SCNs. After that point, the release rate slowed down; in addition, the amount of etoposide released from the ESCNs occurred in the following order: pH 3.0 > pH 5.8 > pH 7.4. The faster release of etoposide in acidic conditions (especially in the strong acidic condition) may be due to the acid-degradable nature of SCNs. At a pH of 7.4 the release amount was quite low, and only approximately 23% of the drug was released in 72 hours, with no 'burst effect', which suggests that the delivery process might be primarily governed by diffusion from the outer layer rather than from the degradation of ESCNs. At a pH of 5.8, the release curve leveled off after 39 hours, and the release amount was 66% in 72 hours. It is noted that when the pH decreased to 3.0, a faster release behavior was observed, and the release amount reached 83%

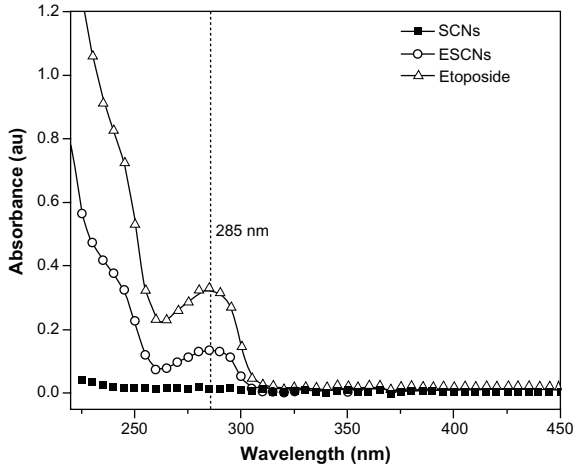


**Figure 5** UV-vis spectra for SCNs, free etoposide and ESCNs.
**Abbreviations:** UV-vis, ultraviolet-visible spectroscopy; SCNs, strontium carbonate nanoparticles; ESCNs, etoposide-loaded strontium carbonate nanoparticles.

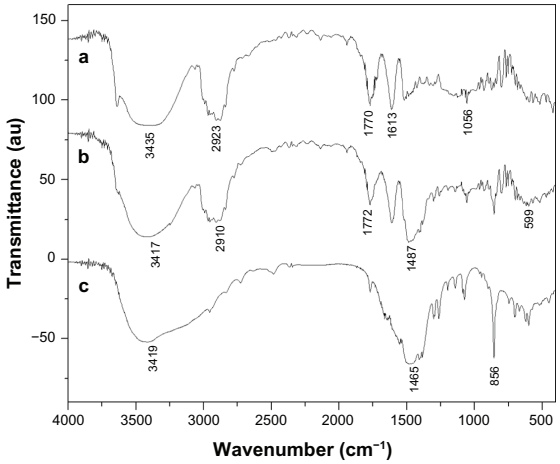


**Figure 6** FTIR spectra for (**a**) free etoposide, (**b**) ESCNs and (**c**) SCNs.
**Abbreviations:** FTIR, Fourier transform infrared spectroscopy; ESCNs, etoposide-loaded strontium carbonate nanoparticles; SCNs, strontium carbonate nanoparticles.

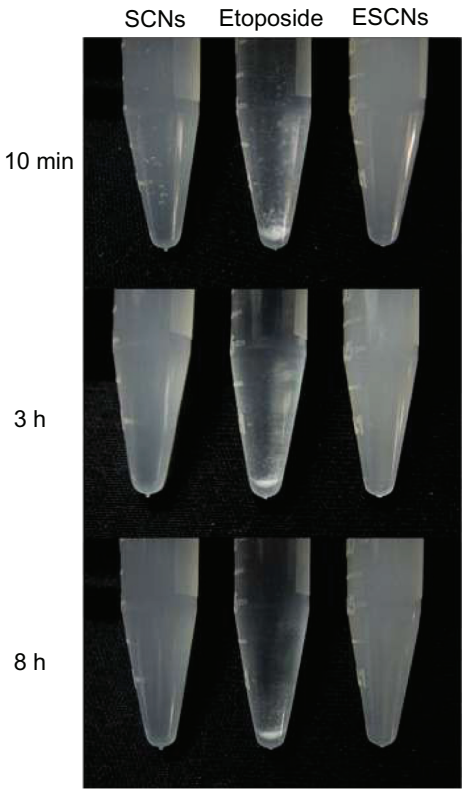


**Figure 7** Sedimentation photographs of SCNs, free etoposide, and ESCNs in double distilled water after standing for 10 minutes, 3 hours, and 8 hours.
**Abbreviations:** SCNs, strontium carbonate nanoparticles; ESCNs, etoposide-loaded strontium carbonate nanoparticles.

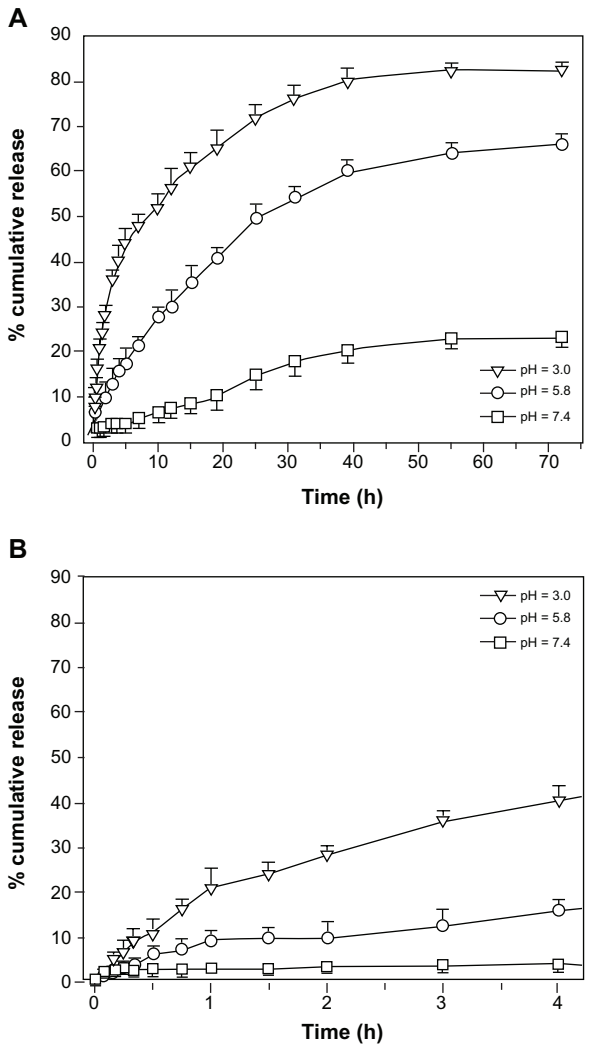


**Figure 8** Release profiles of etoposide from ESCNs under simulated physiological conditions. (**A**) Release profiles of etoposide from ESCNs under simulated physiological conditions (pH 3.0, pH 5.8, and pH 7.4 at 37°C); (**B**) release profiles in the initial 4 hours.
**Note:** All experiments were carried out in triplicate.
**Abbreviation:** ESCNs, etoposide-loaded strontium carbonate nanoparticles.

in 72 hours, which was 3.6 times of that at a pH level of 7.4. These results can demonstrate that the engineered ESCNs are a pH-sensitive controlled drug-delivery system, which may be of particular feasibility in achieving gastric tumor-targeted therapy.

Suppose that oral administration is chosen; the ESCNs can be resistant to gastric acids and ensure a stable delivery of etoposide during the brief stay in stomach (typically, 3–4 hours).[40] When the nanohybrids accumulate at the tumor site through the EPR effect upon circulation in the blood vessels, a fast and stable etoposide release can be triggered in response to extracellular or intracellular chemical stimulation of tumor cells, where the pH value is lower than in the normal tissue. As a result, a gastric cancer treatment is expected to be carried out in multiple ways through a targeted and safe method of delivery, with minimal side effects.

The pH-buffering properties of SCNs, etoposide, and ESCNs were tested by a titration method. The correlation between pH value and added volume of a 0.1 M HCl solution is shown in Figure 9. The pH curves of both SCNs and ESCNs revealed that there was a profound buffer effect as the pH value was maintained at around 6.0 with the addition of a few mL of a 0.1 M HCl solution, while etoposide presented with a poor buffering property; this could be explained by the fact that strontium carbonate is acid-degradable. A three-phase release process can be observed. At the first stage, with the addition of 0.1 M HCl, the scaly exfoliation of SCNs was made by HCl to induce the destruction of the integrity of the coating layer, which resulted in a sharp decrement of the solution pH from about 8 to 6. Along with the degradation of ESCNs as the strontium carbonate in nanoparticles reacted with the HCl, the pH of the medium solution was maintained at about 6 (at the intermediate stage), which was dependent on the neutralization value of SCNs. At the last stage, the pH of the medium solution was cut down and was reduced to 2, as the strontium carbonate in the nanoparticles

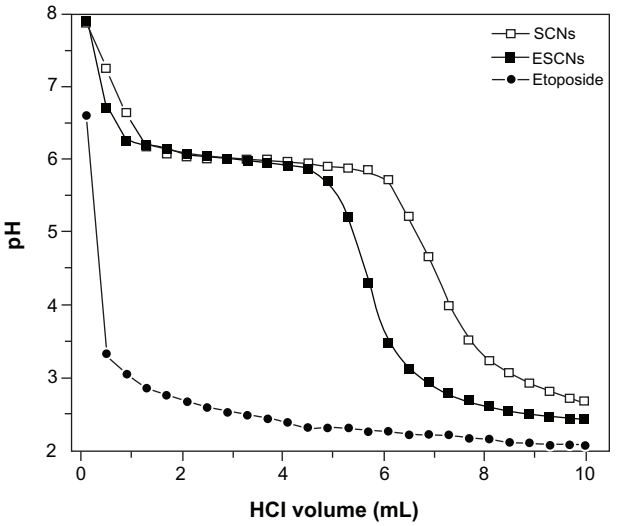


**Figure 9** Titration curves of SCNs, free etoposide, and ESCNs.
**Note:** The abscissa represents the added volume of a 0.1 M HCl aqueous solution.
**Abbreviations:** SCNs, strontium carbonate nanoparticles; ESCNs, etoposide-loaded strontium carbonate nanoparticles.

was consumed by HCl. Compared with SCNs, the ESCNs can dissolve fast since their structure was mixed with the drug, etoposide. In effect, ESCNs are more easily dissolved, which further reduces the buffering effect. Nevertheless, ESCNs may significantly buffer the drug microclimate in gastric fluids compared with free etoposide.

Figure 10A and B show the viability of HEK293T cells treated with SCNs, free etoposide, and ESCNs at various concentrations for 24 and 48 hours, respectively. The average residual HEK293T cells remained over 90% after being incubated with SCNs for 48 hours, even at the highest tested dose, indicating that SCNs were highly biocompatible with HEK293T cells. Compared with free etoposide, ESCNs presented no obvious cytotoxicity against normal cells. The data reveals the good biocompatibility and stable drug-loading effect of the nanocarriers.

Figure 10C and D show the effect of etoposide formulation on the inhibition against SGC-7901 cell growth. Time-dependent inhibition of SGC-7901 cells treated with the samples was indicated. With increased incremental treatment durations, the viability of SGC-7901 cells was reduced. The order of the inhibitory efficacy on SGC-7901 cells was ESCNs > etoposide > SCNs. The rationale behind this order can be explicated below. Good dispersion of ESCNs in an aqueous solution facilitates greater cellular uptake than that of free etoposide. Furthermore, with a sustained release of drug triggered in the acidic microenvironment of SGC-7901 cells, ESCNs can make the most efficient delivery of etoposide into the tumor cells. After treatment with ESCNs over 48 hours, the average residual SGC-7901 cells were about 17% among the control group. This value was about one-third of the percentage of the number of SGC-7901 cells treated with the free etoposide solution. Synergistic therapeutic effects occurred when etoposide combined with SCNs. In parallel, the empty nanoparticles demonstrated no significant inhibitory effect.

Results of the apoptosis assay after staining cells with annexinV-FITC, using PI labeling, and using FACS for determining the percentages of early and late apoptotic cells are illustrated in Figure 11. Early apoptosis was characterized by plasma membrane reorganization and was detected by positive staining for annexin V-FITC, while later stage apoptosis indicating DNA damage showed positive staining for both annexin V and PI.[41] SGC-7901 cells were treated with 10 μg/mL of ESCNs as well as with free etoposide for 24 hours prior to FACS analysis; meanwhile, cells without any additives were set as controls. As shown in Figure 11A, SGC-7901 cells without any additives showed 0.17% early apoptosis and 0.20% later apoptosis. The treatment with etoposide led to early apoptosis in 8.95% of cells, and to later apoptosis in 2.06% of cells (Figure 11B). Remarkably, the percentage of cells that reached early apoptosis increased to 29.38%, and the percentage of cells that reached later apoptosis increased to 5.20% (Figure 11C) when the cells were treated with ESCNs.

Etoposide can cause apoptosis cascade in gastric cancer cells by coupling DNA damage to p53 phosphorylation through the action of DNA-dependent protein kinase. As the activation of p53 increases, Bax synthesis and the translocation of Bax to the mitochondria induces the mitochondrial permeability transition, the event that releases cytochrome c and culminates in the death of the cells.[42] The percentage of both early apoptosis and later apoptosis in ESCNs is significantly increased compared with free etoposide and untreated controls, which confirms that ESCNs were able to induce the apoptosis processes among gastric cancer cells and readily caused the cells to die. Therefore, ESCNs may be more readily taken up by SGC-7901 cells and could protect etoposide from rapid decomposition. The results also prove that etoposide entrapped in SCNs can enhance the anticancer efficiency of the drug and serve as excellent vehicles for anticancer drug release.

The tumor targeting process of pH-sensitive ESCNs in the body may be conjectured as follows (scheme shown in Figure 12). As tumor vessels are often dilated and fenestrated with an average pore size of less than 1 μm compared with normal tissue due to rapid formation of

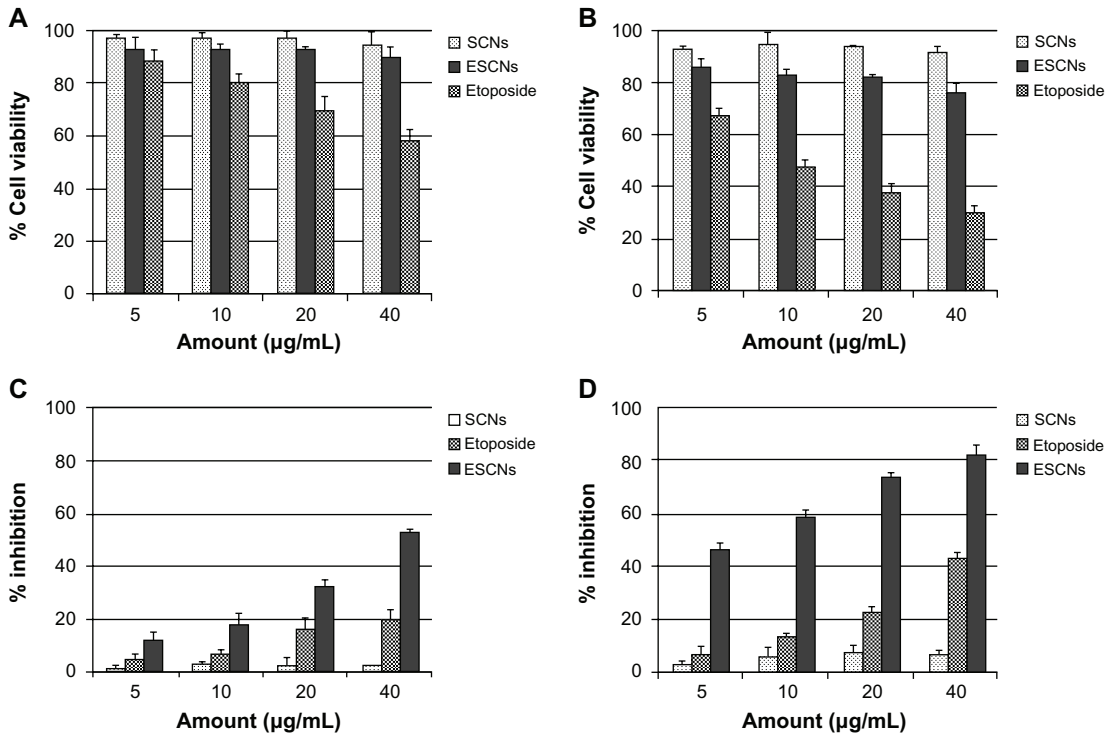


**Figure 10** (**A** and **B**) Growth inhibition assay results for HEK293T cell line with SCNs, free etoposide, and ESCNs after 24 and 48 hours of incubation. Graphs were plotted as particle concentrations of 5, 10, 20, and 40 μg/mL, respectively; (**C** and **D**) growth inhibition assay results for the SGC-7901 cell line with SCNs, free etoposide, and ESCNs after 24 and 48 hours of incubation.

**Notes:** Graphs were plotted as etoposide concentrations of 5, 10, 20, and 40 μg/mL, respectively. All experiments were carried out in triplicate.

**Abbreviations:** SCNs, strontium carbonate nanoparticles; ESCNs, etoposide-loaded strontium carbonate nanoparticles.

vessels that must serve the fast-growing tumor,[43] the nanoscale size enables ESCNs to leave the tumor vasculature through the leaky endothelial tissue and then accumulate in solid tumors by the EPR effect, while normal tissues contain capillaries with tight junctions that are less permeable to nanosized particles.[1] After that, rapid and sustained release of etoposide from ESCNs is triggered in response to low pH in relatively acidic extracellular fluids in the tumor, or after endocytosis in the endosomes or lysosomes in tumor cells, together with the degradation of the nanocarriers. It should be noted that in this process of tumor targeting, both penetration through blood vessels and cellular internalization of drug-containing particles are likely to play a key role in determining their targeted and biological activity. As reported, these processes result in changes in the size of the particles, rather than binding in the form of "passive targeting."[44] In most studies, tumors exhibited a vascular pore cutoff size ranging from 400 nm to 800 nm,

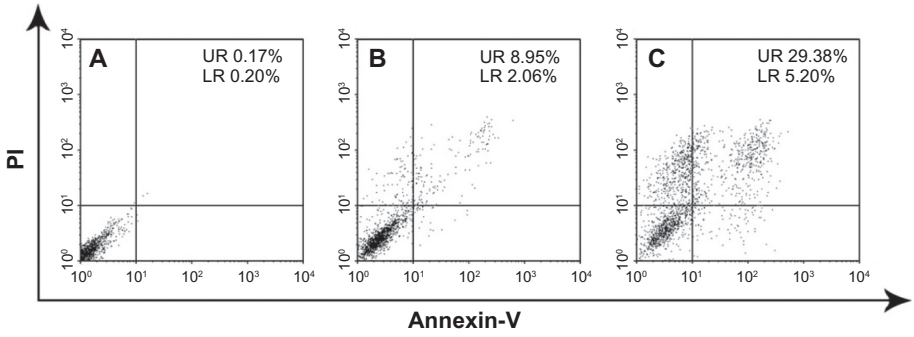


**Figure 11** FACS analysis of SGC-7901 cells stained with Annexin V-FITC and PI. (**A**) Cells were not treated with any agents for blank control; (**B**) apoptotic cells were induced by etoposide, (**C**) cells treated with the ESCNs.

**Note:** In all panels, LR represents early apoptosis and UR represents late apoptosis.

**Abbreviations:** FACS, fluorescence-activated cell sorting; PI, propidium iodide; ESCNs, etoposide-loaded strontium carbonate nanoparticles; LR, low right quadrant; UR, up right quadrant.

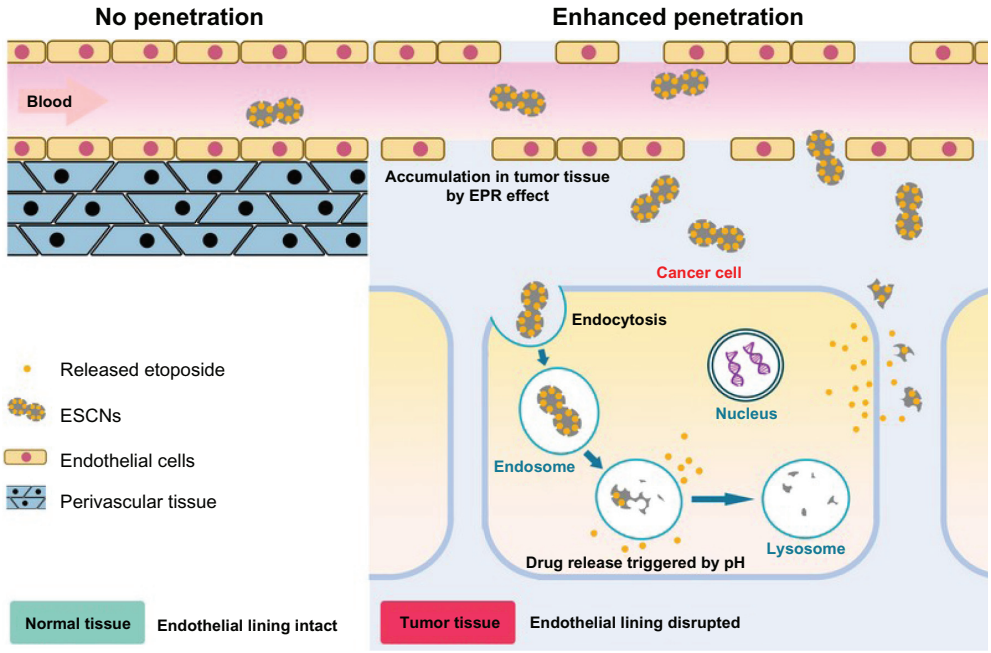


**Figure 12** A representative illustration of pH-sensitive ESCNs targeting.
**Abbreviations:** ESCNs, etoposide-loaded strontium carbonate nanoparticles; EPR, enhanced permeability and retention.

and permeability to a particle is independent of pore cutoff size as long as the diameter of the particle is much less than the pore diameter.[45]

Studies have shown that particles with diameters less than 200 nm are small enough to avoid nonselective uptake by macrophages of the reticuloendothelial system,[46] and are more effective when they accumulate at the tumor site via the EPR effect upon circulation in the blood vessels.[47,48] Also, conclusions have been drawn that nanoparticles with a diameter of less than 200 nm may determine the almost exclusive internalization along the pathway of clathrin-coated pits rather than via caveolae.[49] These results suggest that the engineered pH-sensitive ESCNs with a size of 86.8 nm might have great potential in cancer therapy, for their capability of permeation and retention within the tumor region can be enhanced due to their favorable size. Further in vivo delivery of ESCNs in an animal model will be performed to verify this conjecture.

## Conclusion

SCNs were initially designed and engineered as nanocarriers via a biologically and environmentally favorable one-step mixed solvent method with citric acid as a crystal modifier, aimed at producing high efficiency in tumor-selective drug delivery. The dumbbell-shaped nanoparticles of a uniform size (86.8 nm) present a good dispersivity in aqueous solution. Etoposide as a model drug was successfully entrapped into ESCNs based on a simultaneous process that both the formation of the nanocarriers and the storage of the drug were accomplished in a single step, and the ESCNs possessed both a high loading capacity (34.4%) and encapsulation efficiency (71.6%). The cumulative release of etoposide from the nanocarriers showed a low leakage at pH 7.4 with only 23% of the drug released after 72 hours, while this rate was significantly enhanced to 66% at a pH of 5.8, and 83% at a pH of 3.0. These results demonstrated that the drug release of ESCNs was likely pH-sensitive. The cytotoxicity test and apoptosis test showed that the blank carrier SCNs were almost nontoxic, and the ESCNs were evidently more potent in antitumor activity when compared with free etoposide. These results indicated that the SCNs hold great promise for the development of efficient and selective tumor therapy. These promising results encourage us to perform further in vivo delivery of drugs in an animal model in the future.

## Acknowledgments

This work was financially supported by the 973 project of the Ministry of Science and Technology (Grant No 2010CB912604, 2010CB933901), the National Natural Science Foundation of China (Grant No 31140038), International Science and Technology Cooperation Program of China, (Grant No 0102011DFA32980), Science and Technology Commission of Shanghai Municipality (Grant No 11411951500), and the Fundamental Research Funds for the Central Universities.

## Disclosure

The authors report no conflict of interest in this work.

## References


1. Maeda H, Wu J, Sawa T, Matsumura Y, Hori K. Tumor vascular permeability and the EPR effect in macromolecular therapeutics: a review. *J Control Release*. 2000;65(1–2):271–284.
2. Ferrari M. Cancer nanotechnology: opportunities and challenges. *Nat Rev Cancer*. 2005;5(3):161–171.
3. Jones D. Cancer nanotechnology: small, but heading for the big time. *Nat Rev Drug Discov*. 2007;6(3):174–175.
4. Kaminskas LM, McLeod VM, Kelly BD, et al. A comparison of changes to doxorubicin pharmacokinetics, antitumor activity, and toxicity mediated by PEGylated dendrimer and PEGylated liposome drug delivery systems. *Nanomedicine*. 2012;8(1):103–111.
5. Studenovsky M, Ulbrich K, Ibrahimova M, Rihova B. Polymer conjugates of the highly potent cytostatic drug 2-pyrrolinodoxorubicin. *Eur J Pharm Sci*. 2011;42(1–2):156–163.
6. Ho KS, Aman AM, Al-awar RS, Shoichet MS. Amphiphilic micelles of poly(2-methyl-2-carboxytrimethylene carbonate-co-D,L-lactide)-graft-poly(ethylene glycol) for anti-cancer drug delivery to solid tumours. *Biomaterials*. 2012;33(7):2223–2229.
7. Huynh VT, Quek JY, de Souza PL, Stenzel MH. Block copolymer micelles with pendant bifunctional chelator for platinum drugs: effect of spacer length on the viability of tumor cells. *Biomacromolecules*. 2012;13(4):1010–1023.
8. Yavuz MS, Cheng Y, Chen J, et al. Gold nanocages covered by smart polymers for controlled release with near-infrared light. *Nat Mater*. 2009;8(12):935–939.
9. Knezevic NZ, Slowing II, Lin VS. Tuning the release of anticancer drugs from magnetic iron oxide/mesoporous silica core/shell nanoparticles. *Chempluschem*. 2012;77(1):48–55.
10. Berlin JM, Leonard AD, Pham TT, et al. Effective drug delivery, in vitro and in vivo, by carbon-based nanovectors noncovalently loaded with unmodified paclitaxel. *ACS Nano*. 2010;4(8):4621–4636.
11. Zhu RR, Qin LL, Wang M, et al. Preparation, characterization, and anti-tumor property of podophyllotoxin-loaded solid lipid nanoparticles. *Nanotechnology*. 2009;20(5):055702.
12. Hosseinzadeh H, Atyabi F, Dinarvand R, Ostad SN. Chitosan-Pluronic nanoparticles as oral delivery of anticancer gemcitabine: preparation and in vitro study. *Int J Nanomedicine*. 2012;7:1851–1863.
13. Wang WR, Zhu RR, Xie Q, et al. Enhanced bioavailability and efficiency of curcumin for the treatment of asthma by its formulation in solid lipid nanoparticles. *Int J Nanomedicine*. 2012;7:3667–3677.
14. Li Y, Xiao W, Xiao K, et al. Well-defined, reversible boronate crosslinked nanocarriers for targeted drug delivery in response to acidic pH values and cis-diols. *Angew Chem Int Ed Engl*. 2012;51(12):2864–2869.
15. Huang C, Tang Z, Zhou Y, et al. Magnetic micelles as a potential platform for dual targeted drug delivery in cancer therapy. *Int J Pharm*. 2012;429(1–2):113–122.
16. Lee ES, Gao Z, Bae YH. Recent progress in tumor pH targeting nanotechnology. *J Control Release*. 2008;132(3):164–170.
17. Bae Y, Jang WD, Nishiyama N, Fukushima S, Kataoka K. Multifunctional polymeric micelles with folate-mediated cancer cell targeting and pH-triggered drug releasing properties for active intracellular drug delivery. *Mol Biosyst*. 2005;1(3):242–250.
18. Gillies RJ, Raghunand N, Karczmar GS, Bhujwalla ZM. MRI of the tumor microenvironment. *J Magn Reson Imaging*. 2002;16(4):430–450.
19. Johnson RP, Jeong YI, Choi E, et al. Biocompatible poly(2-hydroxyethyl methacrylate)-b-poly(L-histidine) hybrid materials for pH-sensitive intracellular anticancer drug delivery. *Adv Funct Mater*. 2012;22(5):1058–1068.
20. Lin W, Kim D. pH-Sensitive micelles with cross-linked cores formed from polyaspartamide derivatives for drug delivery. *Langmuir*. 2011;27(19):12090–12097.
21. Li Y, Heo HJ, Gao GH, et al. Synthesis and characterization of an amphiphilic graft polymer and its potential as a pH-sensitive drug carrier. *Polymer*. 2011;52(15):3304–3310.
22. Deng Z, Zhen Z, Hu X, Wu S, Xu Z, Chu PK. Hollow chitosan-silica nanospheres as pH-sensitive targeted delivery carriers in breast cancer therapy. *Biomaterials*. 2011;32(21):4976–4986.
23. Jin YH, Hu HY, Qiao MX, et al. pH-sensitive chitosan-derived nanoparticles as doxorubicin carriers for effective anti-tumor activity: preparation and in vitro evaluation. *Colloids Surf B Biointerfaces*. 2012;94:184–191.
24. Roy I, Vij N. Nanodelivery in airway diseases: challenges and therapeutic applications. *Nanomedicine*. 2010;6(2):237–244.
25. Li A, Qin LL, Zhu D, Zhu RR, Wang SL. Signalling pathways involved in the activation of dendritic cells by layered double hydroxide nanoparticles. *Biomaterials*. 2010;31(4):748–756.
26. Sun DM, Zhu DZ, Wu QS. Synthesis and design of MnCO3 crystals with different morphologies by supported liquid membrane. *J Chem Crystallogr*. 2008;38(12):949–952.
27. Sun DM, Wu QS, Ding YP. A novel method for crystal control: synthesis and design of strontium carbonate with different morphologies by supported liquid membrane. *J Appl Crystallogr*. 2006;39:544–549.
28. Li A, Qin LL, Wang WR, et al. The use of layered double hydroxides as DNA vaccine delivery vector for enhancement of anti-melanoma immune response. *Biomaterials*. 2011;32(2):469–477.
29. Xiao R, Wang WR, Pan LL, et al. A sustained folic acid release system based on ternary magnesium/zinc/aluminum layered double hydroxides. *Journal of Materials Science*. 2011;46(8):2635–2643.
30. Terzyk AP, Pacholczyk A, Wisniewski M, Gauden PA. Enhanced adsorption of paracetamol on closed carbon nanotubes by formation of nanoaggregates: carbon nanotubes as potential materials in hot-melt drug deposition-experiment and simulation. *J Colloid Interface Sci*. 2012;376(1):209–216.
31. Shirkhanzadeh M. Microneedles coated with porous calcium phosphate ceramics: effective vehicles for transdermal delivery of solid trehalose. *J Mater Sci Mater Med*. 2005;16(1):37–45.
32. El-Gamel NE, Wortmann L, Arroub K, Mathur S. SiO2@Fe2O3 core-shell nanoparticles for covalent immobilization and release of sparfloxacin drug. *Chem Commun (Camb)*. 2011;47(36):10076–10078.
33. Wu C, Yu C, Chu M. A gold nanoshell with a silica inner shell synthesized using liposome templates for doxorubicin loading and near-infrared photothermal therapy. *Int J Nanomedicine*. 2011;6:807–813.
34. Hsieh DS, Lu HC, Chen CC, Wu CJ, Yeh MK. The preparation and characterization of gold-conjugated polyphenol nanoparticles as a novel delivery system. *Int J Nanomedicine*. 2012;7:1623–1633.
35. Naveau B. Strontium: a new treatment for osteoporosis. *Joint Bone Spine*. 2004;71(4):261–263.
36. Li Z, Peng S, Pan H, Tang B, Lam RW, Lu WW. Microarchitecture and nanomechanical properties of trabecular bone after strontium administration in osteoporotic goats. *Biol Trace Elem Res*. 2012;145(1):39–46.
37. Ha W, Wu H, Wang XL, et al. Self-aggregates of cholesterol-modified carboxymethyl konjac glucomannan conjugate: preparation, characterization, and preliminary assessment as a carrier of etoposide. *Carbohydr Polym*. 2011;86(2):513–519.
38. Jin HY, Xia F, Zhao YP. Preparation of hydroxypropyl methyl cellulose phthalate nanoparticles with mixed solvent using supercritical antisolvent process and its application in co-precipitation of insulin. *Advanced Powder Technology*. 2012;23(2):157–163.
39. Saadati R, Dadashzadeh S. Simple and efficient HPLC-UV quantitation of etoposide and its cis-isomer in rat micro-volume plasma and tissue samples: application to pharmacokinetic and biodistribution studies. *J Liq Chromatogr*. 2011;34(18):2130–2148.
40. Klausner EA, Lavy E, Friedman M, Hoffman A. Expandable gastroretentive dosage forms. *J Control Release*. 2003;90(2):143–162.
41. Lee MK, Lim SJ, Kim CK. Preparation, characterization and in vitro cytotoxicity of paclitaxel-loaded sterically stabilized solid lipid nanoparticles. *Biomaterials*. 2007;28(12):2137–2146.

42. Karpinich NO, Tafani M, Rothman RJ, Russo MA, Farber JL. The course of etoposide-induced apoptosis from damage to DNA and p53 activation to mitochondrial release of cytochrome c. *J Biol Chem*. 2002;277(19):16547–16552.
43. Fahmy TM, Fong PM, Goyal A, Saltzman WM. Targeted for drug delivery. *Mater Today*. 2005;8(8):18–26.
44. Barreto JA, O'Malley W, Kubeil M, Graham B, Stephan H, Spiccia L. Nanomaterials: applications in cancer imaging and therapy. *Adv Mater*. 2011;23(12):H18–H40.
45. Hobbs SK, Monsky WL, Yuan F, et al. Regulation of transport pathways in tumor vessels: role of tumor type and microenvironment. *Proc Natl Acad Sci U S A*. 1998;95(8):4607–4612.
46. Oh JM, Choi SJ, Lee GE, Kim JE, Choy JH. Inorganic metal hydroxide nanoparticles for targeted cellular uptake through clathrin-mediated endocytosis. *Chem Asian J*. 2009;4(1):67–73.
47. Peer D, Karp JM, Hong S, Farokhzad OC, Margalit R, Langer R. Nanocarriers as an emerging platform for cancer therapy. *Nat Nanotechnol*. 2007;2(12):751–760.
48. Maeda H. The enhanced permeability and retention (EPR) effect in tumor vasculature: the key role of tumor-selective macromolecular drug targeting. *Adv Enzyme Regul*. 2001;41:189–207.
49. Rejman J, Oberle V, Zuhorn IS, Hoekstra D. Size-dependent internalization of particles via the pathways of clathrin- and caveolae-mediated endocytosis. *Biochem J*. 2004;377(Pt 1):159–169.